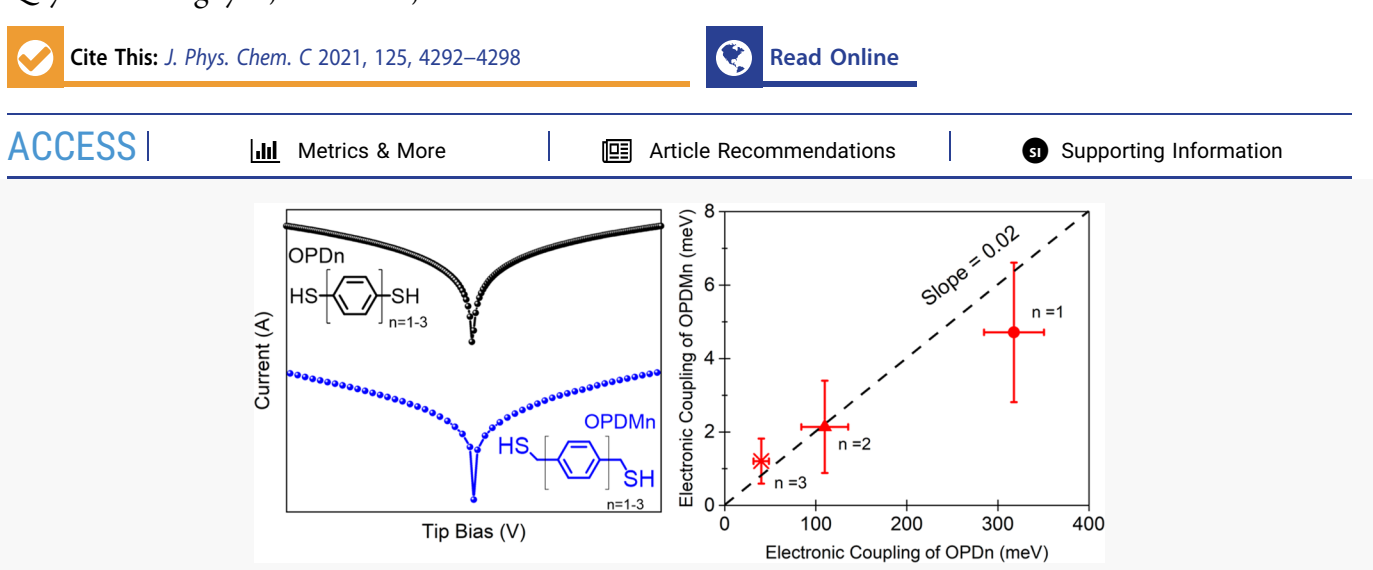


pubs.acs.org/JPCC Article

Quantifying Molecular Structure-Tunneling Conductance Relationships: Oligophenylene Dimethanethiol vs Oligophenylene Dithiol Molecular Junctions

Quyen Van Nguyen, Zuoti Xie, and C. Daniel Frisbie*



ABSTRACT: We report quantitative analysis of tunneling conductance in molecular junctions based on self-assembled monolayers (SAMs) of oligophenylene dimethanethiols (OPDMn) in which $-CH_2$ – spacers flank either side of the phenylene (n = 1), biphenylene (n = 2), and terphenylene (n = 3) aromatic cores. The current–voltage (I-V) characteristics for the OPDMn junctions with Au and Pt contacts are analyzed quantitatively with a previously validated single level model (SLM) to extract key junction metrics, namely the HOMO-to-Fermi-level offset, ε_h , and the electronic coupling, Γ. Independent determination of ε_h by ultraviolet photoelectron spectroscopy (UPS) corroborates the estimation of ε_h from the I-V characteristics and provides strong evidence for the validity of the SLM analysis. Further, comparison of the results for OPDMn junctions with those for oligophenylene dithiol (OPDn) junctions, which do not have $-CH_2$ – spacers, reveals that the much larger resistance for OPDMn (>1000-fold) is primarily due to a ~50-fold decrease in Γ and not to any significant change in ε_h ; ε_h is nearly identical for OPDMn and OPDn junctions for each value of n. Overall, our results provide a clear delineation of the influence of $-CH_2$ – spacers on ε_h and Γ and give further evidence that the analytical SLM is a useful tool for determining structure-transport relationships in molecular tunnel junctions.

■ INTRODUCTION

A central focus of molecular electronics is to understand the effect of chemical structure on electron transport through metal-molecule-metal junctions, 1-33 Figure 1. For symmetric junctions where off-resonant, single-step tunneling dominates, the analytical single level model (SLM) derived from the Landauer picture has proven to be a convenient theoretical tool to determine key transport parameters from junction current–voltage (I-V) characteristics. $^{5-7,9,10,12,13,30}$ These parameters include the HOMO (or LUMO) energy offset, $\varepsilon_{
m h}$ (or ε_1), and the orbital coupling Γ , as shown in Figure 1B. Recent work by Baldea^{34–36} and the authors^{5–8,11–13,30,37} has demonstrated that $\varepsilon_{\rm h}$ and Γ are easily extracted from experimental data using the analytical SLM, and the resulting I-V prediction by SLM matches the experimental I-Vcharacteristics very well. The validity of the SLM for simple tunnel junctions is also corroborated by independent determination of $\varepsilon_{\rm h}$ by ultraviolet photoelectron spectroscopy

(UPS) for oligophenylene thiol and alkanethiol systems, ^{6,7} and by its prediction of "universal" behavior for single-step tunneling that matches experimental findings. ^{5,8,12}

In this paper, we combine experiments and SLM analysis to assess the impact of aliphatic $-\mathrm{CH_2}-$ spacers on ε_h and Γ for junctions based on self-assembled monolayers (SAMs) of oligophenylene dimethanethiols (OPDMn, n=1-3) compared to SAMs of oligophenylene dithiols (OPDn) that do not have the spacer, Figure 1A. Our experiments use the conducting probe atomic force microscopy (CP-AFM) platform. The insertion of an aliphatic spacer is well-known to

Received: December 28, 2020 Revised: February 2, 2021 Published: February 10, 2021





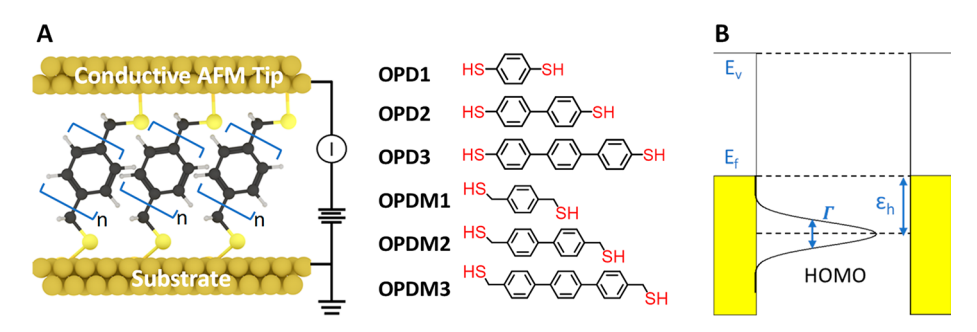


Figure 1. (A) Schematic representation of a metal-molecule-metal junction. To make the junction, a metal-coated AFM tip is brought into contact with a SAM of OPDMn or OPDn on Au or Pt substrates. Molecular structures of OPDn and OPDMn (n = 1-3) are shown. (B) Typical junction electronic structure with main parameters $ε_h$ and Γ.

produce a dramatic decrease in molecular conductance generally. 17,38,39 Our goal is not to simply confirm that this is so but rather to understand the quantitative impact on the $\varepsilon_{\rm h}$ and Γ metrics extracted by SLM analysis. The utility of SLM for understanding the physical organic chemistry of molecular conductance will ultimately depend on having self-consistent measurements of $\varepsilon_{\rm h}$ and Γ on a wide range of molecules as a function of their architecture. We thus seek to quantify these metrics for the prototypical case of $-{\rm CH_2}-$ insertion and, simultaneously, to add to the growing body of evidence that the SLM can be applied productively to the analysis of single-step tunneling junctions like those based on OPDMn.

Indeed, we observe here that the SLM I-V simulation for OPDMn junctions matches the measured I-V data, and the $\varepsilon_{\rm h}$ values determined by SLM analysis agree remarkably well with those measured by UPS. We find that introducing $-{\rm CH_2}-$ groups increases OPDMn resistance by 3 orders of magnitude relative to OPDn junctions, and the increased resistance is overwhelmingly attributable to a decrease in the electronic coupling Γ , not to an increase in $\varepsilon_{\rm h}$. Clear delineation of structural influences on $\varepsilon_{\rm h}$ and Γ is a principal result of our study.

We summarize the relevant SLM formulas here. SLM predicts the I-V characteristics for a symmetric junction are described by eq 1

$$I = GV \frac{{\varepsilon_{\rm h}}^2}{{\varepsilon_{\rm h}}^2 - (eV/2)^2} \tag{1}$$

where G is the zero bias conductance that can be expressed as follows

$$G = NG_0 \frac{\Gamma^2}{\varepsilon_h^2} \tag{2}$$

Here, $\Gamma=\sqrt{\Gamma_{\rm s}\Gamma_{\rm t}}=\varepsilon_{\rm h}\sqrt{G/NG_0}$ is the average interface coupling, $\Gamma_{\rm s}$ and $\Gamma_{\rm t}$ are determined by the molecular coupling to the substrate (s) and the tip (t) ($\Gamma_{\rm s}\approx\Gamma_{\rm t}$ in symmetric junctions), $G_0=2e^2/h$ is the quantum conductance, and N is the number of molecules in the junction. To compute Γ of OPDMn and OPDn junctions, we set N=80, a value close to that directly determined from other dithiol-based CP-AFM junctions. ^{6,7,13}

Importantly, eq 1 enables expression of the HOMO energy offset $\varepsilon_{\rm h}$ in terms of the transition voltages $V_{\rm t+}$ and $V_{\rm t-}$ at positive and negative bias polarity as follows:^{8,25}

$$\varepsilon_{\rm h} = 2 \frac{e|V_{\rm t+}V_{\rm t-}|}{\sqrt{{V_{\rm t+}}^2 + 10|V_{\rm t+}V_{\rm t-}|/3 + {V_{\rm t-}}^2}}$$
(3)

which, when $V_{\rm t+} \approx -V_{\rm t-} \approx V_{\rm t}$ for symmetric junctions, simplifies to

$$\varepsilon_{\rm h} = \frac{\sqrt{3} \, e^{|V_{\rm t}|}}{2} \tag{4}$$

Key assumptions underlying eqs 1-4 are (i) that a single orbital, coupled to the contacts, mediates the off-resonant tunneling, (ii) that the line shape of the broadened orbital is Lorentzian, and (iii) that the orbital offset ε_h is larger than the contact coupling strength Γ .

EXPERIMENTAL METHOD

Materials. Gold nuggets (99.999% pure) were purchased from Mowrey, Inc. (St. Paul, MN) and Kurt J. Lesker Co., respectively. Evaporation boats and Cr evaporation rods were secured from R. D. Mathis (Long Beach, CA). Pt and Ti metal for e-beam evaporation were purchased from Kamis, Inc. (Mahopac Falls, NY). Si (100) wafers were acquired from WaferNet (San Jose, CA). AFM tips (DNP-10 Si₃N₄ contact-mode probes) were purchased from Bruker. 1,4-benzenedimethanethiol (OPDM1) 98% and 4,4'-bis(mercaptomethyl)-biphenyl (OPDM2) 97% were purchased from Sigma-Alrich company. [1,1':4',1"-Terphenyl]-4,4"-dimethanethiol (OPDM3) was synthesized following the procedure reported in the SI.

Conducting Tip and Sample Preparation. Contact-mode AFM tips were coated with Au using a thermal evaporator housed in a N₂-filled glovebox (H₂O, O₂ < 0.1 ppm). Then, 500 Å films were deposited at a rate of 0.5–1.0 Å/s on top of a 50 Å Cr adhesion layer and were immediately transferred without exposure to air to another glovebox containing the CP-AFM to carry out the conductance measurements. For Pt-coated AFM tips, 200 Å thick Pt films were e-beam deposited onto tips with a 50 Å Ti adhesion layer, and immediately transferred to the measurement glovebox. The radii of the tips were ~50 nm after metal coating. $^{\rm 13}$

Template-stripped flat metal substrates were employed to grow high-quality SAMs. ^{5–9,12,13,18,30,40} For flat Au substrates, 5000 Å of Au was first deposited onto clean Si wafers in an ebeam evaporator. Si chips (1 cm²) were then glued onto the metal surface using epoxy (EPOTEK 377, Epoxy Technologies, MA). The epoxy layer was cured by placing the wafers in an oven at 120 °C for 1 h. For flat Pt substrates, 3000 Å of Pt was sputter-coated onto a clean Si wafer at a rate of ~3 Å/s. On top of the Pt film, subsequent deposition of 300 Å of Cr

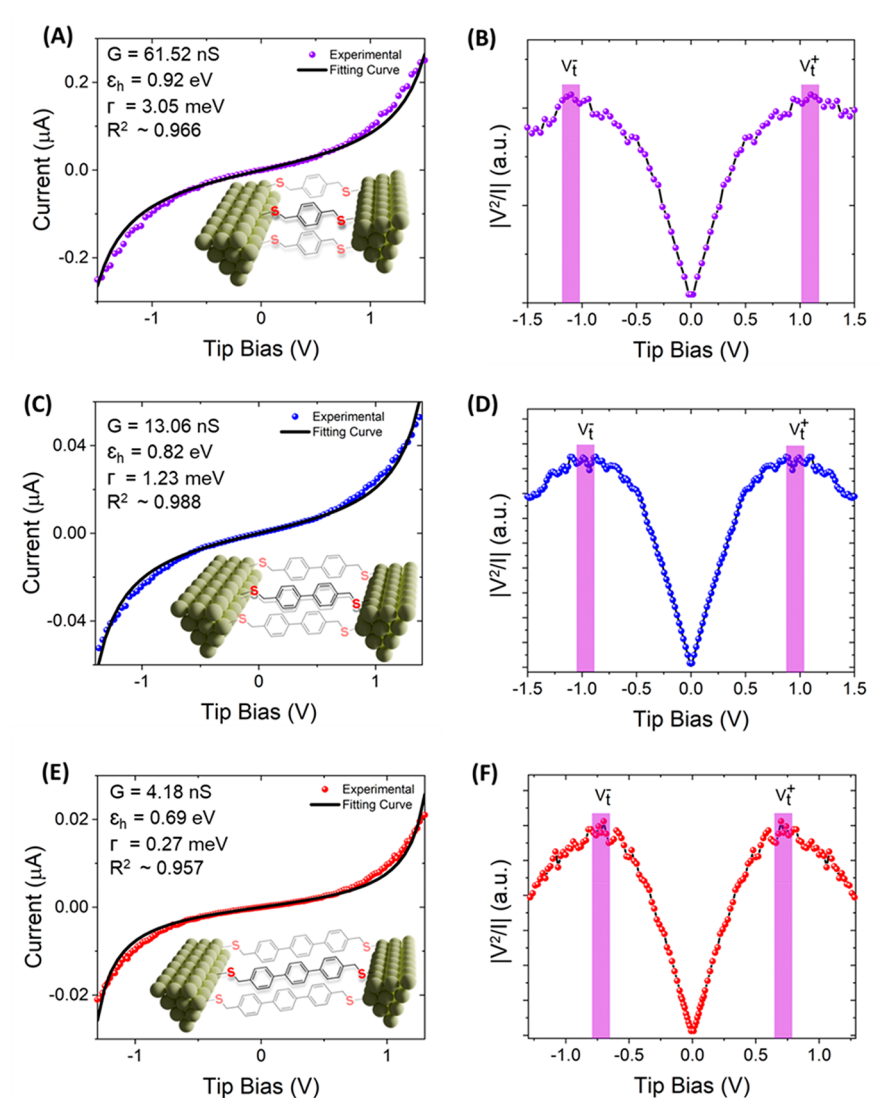


Figure 2. Average I-V curves and transition voltage plots for Au–OPDM1–Au (A, B), Au–OPDM2–Au (C, D), and Au–OPDM3–Au (E, F) tunnel junctions. SLM simulations are shown in black. Extracted parameters for each junction, G, ε_h^{trans} , and Γ , are listed in A, C, and E. G is determined from the low bias slope, ε_h^{trans} is determined from V_t in the transition voltage plots and eq 4, and Γ is computed from G and ε_h^{trans} by eq 2. None of the parameters are freely adjusted.

and 2000 Å of Au was carried out in a thermal evaporator. The Au film enhanced the yield of flat Pt substrates due to better adhesion with the cured epoxy layer.^{6,7,30} The rest of the steps were the same as for flat Au substrates. The flat substrates peeled off the silicon surface were used for SAMs preparation.

To create SAMs, the flat substrate peeled off was incubated in a 0.5 mM hexane solution of the dithiols at 60 $^{\circ}$ C for 1 h in the absence of light. ^{41–44} Afterward, the samples were rinsed with hexane and then ethanol and dried in a stream of N₂ gas.

XPS and UPS Methods. The chemical composition and thickness of the OPDMn SAMs were characterized by XPS (see Supporting Information). The XPS measurements were performed on a PHI Versa Probe III XPS system (ULVAC-PHI) using a monochromatized Al $K\alpha$ X-ray source (1486.6 eV). The base pressure was 5.0×10^{-8} Pa. During data collection, the pressure was ca. 1.0×10^{-6} Pa. The samples were mounted on a piece of double-sided adhesive tape on a sample holder. The samples were grounded by a metal spring clip on the sample holder. The X-ray spot size (diameter) was 200 μ m and the source power was 50 W at 15 kV. Two spots

on the sample were surveyed and the high-resolution C_{1s} and S_{2p} spectra were collected on the second spot. The binding energy scales were referenced to the $Au_{4f7/2}$ peak (84.0 eV).

Angle-resolved XPS (ARXPS) was employed to measure SAM thicknesses on Au and Pt substrates using similar instrument settings with takeoff angles of 20°, 30°, 40°, 50°, 60°, 70°, 80°, and 90°. The HOMO–Fermi level offset of OPDMn SAMs on metals was measured by UPS in the same instrument (section S3 in the Supporting Information).

Transport Measurements. CP-AFM-based molecular junctions were fabricated by mounting the substrates in the AFM and bringing the metal-coated tip into contact with the SAM under a 1 nN applied compressive load. Voltages V were applied to the tip with a Keithley model 236 electrometer operated in sweep mode with the sample grounded. Voltage spanned ± 1.3 V for OPDMn junctions. The slope of the lowbias I-V characteristic (linear portion within the bias range of ± 0.1 V) was used to define a junction (low-bias) conductance G. All transport measurements were carried out in an Ar-filled glovebox (MBraun).

Table 1. Comparison of Key Electronic Structure Parameters, Including the Energy Offset ε_h^{trans} and ε_h^{UPS} , Low Bias Conductance G, and Average Coupling Γ , for OPDn and OPDMn Junctions^a

metal	quantity	OPD1	OPD2	OPD3	OPDM1	OPDM2	OPDM3
Au	$arepsilon_{ m h}^{ m trans}$ (eV)	0.87 ± 0.07	0.73 ± 0.05	0.56 ± 0.04	0.96 ± 0.12	0.88 ± 0.10	0.69 ± 0.11
	$arepsilon_{ m h}^{ m UPS}$ (eV)	0.82 ± 0.10	0.74 ± 0.10	0.68 ± 0.10	1.05 ± 0.10	0.91 ± 0.10	0.81 ± 0.10
	G(S)	1.7×10^{-4}	3.7×10^{-5}	6.7×10^{-6}	$7.4 \pm 2.5 \times 10^{-8}$	$1.4 \pm 0.9 \times 10^{-8}$	$4.4 \pm 1.5 \times 10^{-9}$
	Γ (meV)	141.6 ± 20.8	56.6 ± 8.9	18.3 ± 4.2	3.3 ± 1.3	1.0 ± 0.6	0.7 ± 0.2
Pt	$arepsilon_{ m h}^{ m trans}$ (eV)	0.75 ± 0.08	0.63 ± 0.06	0.49 ± 0.05	0.73 ± 0.11	0.61 ± 0.13	0.5 ± 0.11
	$arepsilon_{ m h}^{ m UPS}$ (eV)	0.81 ± 0.10	0.72 ± 0.10	0.60 ± 0.10	0.71 ± 0.10	0.68 ± 0.10	0.59 ± 0.10
	G(S)	1.1 ± 10^{-3}	1.9×10^{-4}	4.2×10^{-5}	$2.6 \pm 1.3 \times 10^{-7}$	$8.1 \pm 3.6 \times 10^{-8}$	$4.4 \pm 1.8 \times 10^{-8}$
	Γ (meV)	317.6 ± 32.9	109.8 ± 25.4	40.1 + 8.5	4.7 ± 1.9	2.6 ± 1.1	1.2 ± 0.6

^aQuoted errors are the standard deviations, or, in the case of UPS, the estimated accuracy.

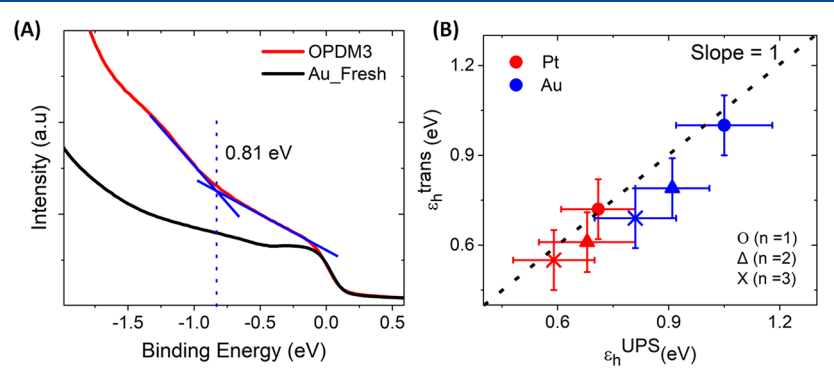


Figure 3. (A) UPS spectra of bare Au and OPDM3 SAMs on Au at low binding energy. Binding energies are referenced to the Fermi level, $E_{\rm ref} = E_{\rm F} = 0$ eV. The blue intersecting lines indicate the onset energy of the HOMO. (B) Comparison of $\varepsilon_{\rm h}^{\rm trans}$ from transport measurements (and the single-level model) with $\varepsilon_{\rm h}^{\rm UPS}$ for OPDMn molecular junctions with Au and Pt contacts.

RESULTS AND DISCUSSION

Formation of OPDMn SAMs. SAMs of aryldimethanethiols have been reported previously. 41–48 We found that OPDMn SAMs could be formed reproducibly on Au and Pt substrates by incubation of the metal surfaces in 0.5 mM *n*-hexane solutions for 1 h at 60 °C in the absence of light. 41–43,45–47,49 The SAMs were characterized by angle resolved X-ray photoelectron spectroscopy (XPS, see section S1 in the Supporting Information, SI).

Transport Behavior for OPDMn Junctions and SLM **Analysis.** Figure 2 displays the I-V characteristics for OPDM1, OPDM2, and OPDM3 junctions with Au contacts, respectively, over $\pm 1.5 \text{ V}$ ($\pm 1.3 \text{ V}$ in the case of OPDM3) and the associated transition voltage (V_t) plots. $^{5-8,12,13}$ The same data set with Pt contacts is shown in Figure S5 in the SI. From the positive (or negative) maximum in each V_t plot we determined $\varepsilon_{\rm h}^{\rm trans}$ (i.e., $\varepsilon_{\rm h}$ from transport) via eq 4. Conductance G was determined from the slope at zero bias. With G and $\varepsilon_h^{\text{trans}}$ as inputs to eq 1, the SLM I-V simulations were made and are shown as the black curves in Figure 2A-C. Comparison of the experimental data with the SLM results is quite satisfactory. Note that Γ is determined from N, G, and $\varepsilon_{\rm h}^{\rm trans}$ via eq 2, but N is taken to be fixed and Γ is not an adjustable parameter in the SLM prediction; it follows directly from determination of G and $\varepsilon_{\rm h}^{\rm trans}$. Furthermore, the SLM predictions (black traces) in Figure 2 are not fits in the conventional sense of having two freely adjustable parameters. Both G and $\varepsilon_{\rm h}^{\rm trans}$ are determined by prescribed procedures just mentioned and then input into eq 1 to yield the simulated I-Vcharacteristic. Table 1 shows the extracted values of G, ε_h^{trans} , and Γ for OPDM1-3 with Au and Pt contacts. Also shown for

comparison are the same metrics for OPD1-3 junctions that have been reported by us previously.^{7,30}

To corroborate the $arepsilon_{
m h}^{
m trans}$ values extracted from the $I\!-\!V$ characteristics for OPDMn, we undertook measurements of $\varepsilon_{\rm h}$ by UPS. Figure 3a displays the UPS spectrum of an OPDM3 SAM on Au relative to that of bare Au; the method of estimating $\varepsilon_h^{\text{UPS}}$ is also shown.^{6,7} As is evident, the HOMO edge is at 0.81 eV, within error in reasonable correspondence with $\varepsilon_h^{\text{trans}} = 0.69 \text{ eV}$ obtained from transport measurements (see Figure 2E). Corresponding UPS spectra for OPDM1 and OPDM2 on Au and Pt substrates are shown in Figure S6 and S7 in the SI; Table 1 also summarizes the $\varepsilon_h^{\text{UPS}}$ values for OPDMn and OPDn (reported earlier) on Au and Pt. Importantly, Figure 3b plots $\varepsilon_{\rm h}^{\rm trans}$ vs $\varepsilon_{\rm h}^{\rm UPS}$ for OPDMn molecules with Au and Pt contacts. One observes that as nincreases, both $\varepsilon_h^{\rm trans}$ and $\varepsilon_h^{\rm UPS}$ decrease as expected because of the increased π -system conjugation. An excellent linear correlation is observed between $arepsilon_h^{\rm trans}$ and $arepsilon_h^{\rm UPS}$ with all of the data following on, or very close, to the slope = 1 guide to the eye. This correlation between the transport-extracted $\varepsilon_{\rm h}$ and $\varepsilon_{\rm h}$ determined independently by electron spectroscopy provides strong additional support for the validity of the SLM for OPDMn junctions.

We note that $\varepsilon_h^{\text{trans}}$ and $\varepsilon_h^{\text{UPS}}$ agree well in spite of the fact that the UPS measurement probes only "half the junction" (i.e., there is no second contact), and this has important implications for the mechanism of energy level alignment. Evidently, binding of an OPDMn molecule to a metal via a single thiol group essentially fixes ε_h ; introducing a second, chemically or physically bonded metal contact has a minimal impact on ε_h . This finding corroborates our earlier reports on different molecular systems ^{6,7} and implies that image charge

effects must be reasonably small, as the effects of a second contact appear to be roughly negligible.

Comparison of OPDMn and OPDn Junctions. Figure 4 displays a direct comparison between the I-V behavior for

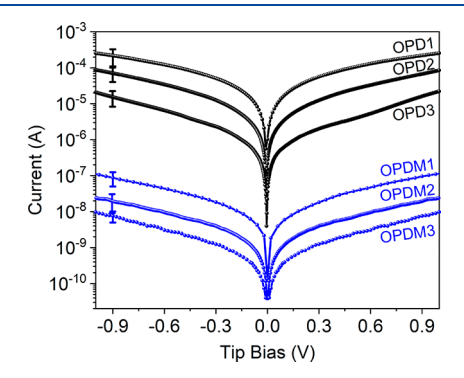


Figure 4. Overlay of semilog plots of average I-V curves for Au-OPDMn-Au (blue) and Au-OPDn-Au (black) junctions.

OPDMn and OPDn junctions with Au contacts. Similar comparative data with Pt contacts are shown in Figure S8. It is clear that OPDMn junctions are approximately 10^3 times less conductive than OPDn junctions at any voltage. The difference can be traced to large differences in G; inspection of Table 1 shows that G for OPDMn is indeed of order $\sim 10^3$ smaller than G for OPDn. As G depends on Γ^2/ε_h^2 (eq 2) it is reasonable to ask which factor, Γ or ε_h , is responsible. Figure 5A plots $\varepsilon_h^{\rm trans}$ for OPDMn vs $\varepsilon_h^{\rm trans}$ for OPDMn. One sees that the correlation is very good; as $\varepsilon_h^{\rm trans}$ for OPDMn increases with decreasing n, $\varepsilon_h^{\rm trans}$ for OPDn also increases approximately commensurately. There is only a very small difference between $\varepsilon_h^{\rm trans}$ for OPDMn and OPDn for any value of n. In other words, insertion of the $-{\rm CH}_2-$ spacer at either end of the OPDMn molecule has not strongly affected $\varepsilon_h^{\rm trans}$, and differences in $\varepsilon_h^{\rm trans}$ cannot be the cause of the very different current levels.

However, Figure 5B reveals a much different story for Γ . The plot of Γ for OPDMn vs OPDn shows very clearly that while Γ correlates for OPDMn and OPDn, the slope of the data set is much less than 1 and is close to 0.02. In other words, for any value of n, Γ for OPDMn is about 50 times smaller than Γ for OPDn. Because G is proportional to Γ^2 , the factor of 50 difference translates to a factor of 2500 in the low bias conductance, which explains the very large difference in currents for OPDMn vs OPDn at any voltage. Thus, the

impact of the $-CH_2-$ spacers on OPDMn conductance is overwhelmingly due to the spacer influence on Γ . At a general level this is an expected result, but it is important that quantitative measures for both ε_h^{trans} and Γ are so easily obtained with the analytical SLM model, and that the relative contributions of ε_h^{trans} vs Γ can be delineated.

The weak dependence of $\varepsilon_{\rm h}^{\rm trans}$ on the presence or absence of the spacers is a more subtle question and likely requires better understanding of the degree of equilibrium charge exchange between the OPDMn and OPDn molecules, respectively, and the metal contacts. That is, at equilibrium OPDMn and OPDn junctions achieve nearly the same equilibrium HOMO offset $\varepsilon_{\rm h}$, which may reflect local charge shifts at the Au–S (or Pt–S) contacts, or between the pi-systems and the contacts, or both effects. Quantum chemical calculations are necessary for further insight on the energy level alignment problem.

CONCLUSION

We have demonstrated here that the analytical single level model can be employed productively to analyze the I-V characteristics of OPDMn molecular junctions and in particular to extract quantitative values for the key metrics $\varepsilon_{\rm h}$ and Γ . Direct comparison of the OPDMn results with SLM results for OPDn junctions, which do not have $-{\rm CH_2}-$ spacers flanking the pi-cores, allowed evaluation of the impact of the spacers on $\varepsilon_{\rm h}$ and Γ . We find that Γ is strongly determined by the spacers but that $\varepsilon_{\rm h}$ is essentially independent of their presence or absence. This information naturally provides a more complete physical description of tunneling conductance in OPDMn versus OPDn junctions.

More generally, our results provide additional evidence that the SLM is a useful model for analysis of junctions in which off-resonance, single-step tunneling applies. We have argued previously^{5–10,12} that for the experimentalist having a simple analytical tool is a tremendous advantage because it allows quantitative structure—property comparisons to be made straightforwardly, and this in turn should enhance conductance assessments of a broader range of molecular structures.

ASSOCIATED CONTENT

Supporting Information

The Supporting Information is available free of charge at https://pubs.acs.org/doi/10.1021/acs.jpcc.0c11514.

Details of OPDM3 synthesis, XPS/UPS data, and I-V curves of Pt/OPDMn/Pt junctions (PDF)

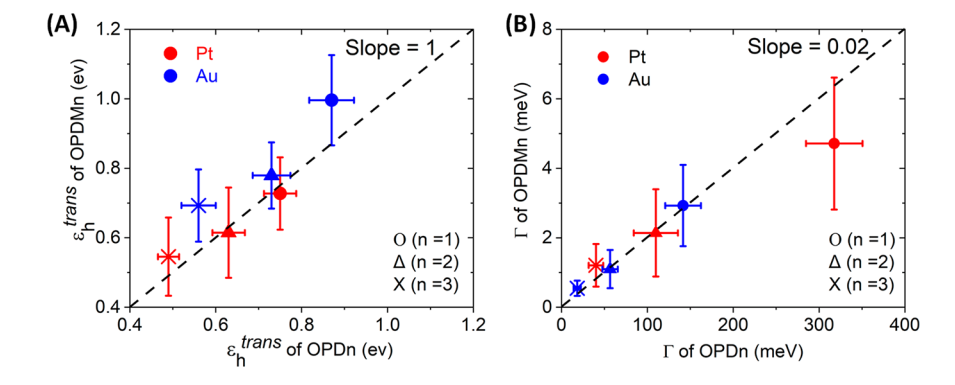


Figure 5. (A) Energy offset $ε_h^{trans}$ of OPDMn vs OPDn junctions as a function of molecular length with Au contacts and Pt contacts. (B) The coupling Γ for OPDMn vs OPDn (n = 1-3) with Au and Pt contacts. $ε_h^{trans}$ and Γ were extracted from I-V characteristics using the single-level model.

AUTHOR INFORMATION

Corresponding Author

C. Daniel Frisbie – Department of Chemical Engineering and Materials Science, University of Minnesota, Minneapolis, Minnesota 55455, United States; oorcid.org/0000-0002-4735-2228; Email: frisbie@umn.edu

Authors

Quyen Van Nguyen — Department of Chemical Engineering and Materials Science, University of Minnesota, Minneapolis, Minnesota 55455, United States; orcid.org/0000-0003-0120-0971

Zuoti Xie — Department of Materials Science and Engineering, Guangdong Technion - Israel Institute of Science, Shantou, Guangdong 515063, China; orcid.org/0000-0002-1828-

Complete contact information is available at: https://pubs.acs.org/10.1021/acs.jpcc.0c11514

Notes

The authors declare no competing financial interest.

ACKNOWLEDGMENTS

The authors acknowledge the financial support of the National Science Foundation (CHE-2003199). Parts of this work were carried out in the Characterization Facility, University of Minnesota, which receives partial support from the NSF through the MRSEC (Award Number DMR-2011401) and NNCI programs (Award Number ECCS-2025124).

REFERENCES

- (1) Jeong, H.; Kim, D.; Xiang, D.; Lee, T. High-Yield Functional Molecular Electronic Devices. ACS Nano 2017, 11, 6511–6548.
- (2) Xiang, D.; Wang, X.; Jia, C.; Lee, T.; Guo, X. Molecular-Scale Electronics: From Concept to Function. *Chem. Rev.* **2016**, *116*, 4318–4440
- (3) Nguyen, Q.; Tefashe, U.; Martin, P.; Della Rocca, M. L.; Lafolet, F.; Lafarge, P.; McCreery, R. L.; Lacroix, J.-C. Molecular Signature and Activationless Transport in Cobalt-Terpyridine-Based Molecular Junctions. *Adv. Electron. Mater.* **2020**, *6*, 1901416.
- (4) Han, Y.; Nickle, C.; Zhang, Z.; Astier, H. P. A. G.; Duffin, T. J.; Qi, D.; Wang, Z.; del Barco, E.; Thompson, D.; Nijhuis, C. A. Electric-Field-Driven Dual-Functional Molecular Switches in Tunnel Junctions. *Nat. Mater.* **2020**, *19*, 843–848.
- (5) Xie, Z.; Baldea, I.; Haugstad, G.; Frisbie, C. D. Mechanical Deformation Distinguishes Tunneling Pathways in Molecular Junctions. J. Am. Chem. Soc. 2019, 141, 497–497.
- (6) Xie, Z.; Bâldea, I.; Frisbie, C. D. Energy Level Alignment in Molecular Tunnel Junctions by Transport and Spectroscopy: Self-Consistency for the Case of Alkyl Thiols and Dithiols on Ag, Au, and Pt Electrodes. J. Am. Chem. Soc. 2019, 141, 18182–18192.
- (7) Xie, Z.; Bâldea, I.; Frisbie, C. D. Determination of Energy Level Alignment in Molecular Tunnel Junctions by Transport and Spectroscopy: Self-Consistency for the Case of Oligophenylene Thiols and Dithiols on Ag, Au, and Pt Electrodes. *J. Am. Chem. Soc.* **2019**, *141*, 3670–3670.
- (8) Xie, Z.; Bâldea, I.; Frisbie, C. D. Why One Can Expect Large Rectification in Molecular Junctions Based on Alkane Monothiols and Why Rectification Is So Modest. *Chem. Sci.* **2018**, *9*, 4456–4456.
- (9) Smith, C. E.; Xie, Z.; Bâldea, I.; Frisbie, C. D. Work Function and Temperature Dependence of Electron Tunneling through an N-Type Perylene Diimide Molecular Junction with Isocyanide Surface Linkers. *Nanoscale* **2018**, *10*, 964–975.
- (10) Rodriguez-Gonzalez, S.; Xie, Z.; Galangau, O.; Selvanathan, P.; Norel, L.; Van Dyck, C.; Costuas, K.; Frisbie, C. D.; Rigaut, S.; Cornil,

- J. Homo Level Pinning in Molecular Junctions: Joint Theoretical and Experimental Evidence. *J. Phys. Chem. Lett.* **2018**, *9*, 2394–2394.
- (11) Nguyen, Q. V.; Martin, P.; Frath, D.; Della Rocca, M. L.; Lafolet, F.; Bellinck, S.; Lafarge, P.; Lacroix, J. C. Highly Efficient Long-Range Electron Transport in a Viologen-Based Molecular Junction. J. Am. Chem. Soc. 2018, 140, 10131–10134.
- (12) Xie, Z.; Bâldea, I.; Oram, S.; Smith, C. E.; Frisbie, C. D. Effect of Heteroatom Substitution on Transport in Alkanedithiol-Based Molecular Tunnel Junctions: Evidence for Universal Behavior. *ACS Nano* **2017**. *11*. 569–578.
- (13) Xie, Z.; Bâldea, I.; Demissie, A. T.; Smith, C. E.; Wu, Y.; Haugstad, G.; Frisbie, C. D. Exceptionally Small Statistical Variations in the Transport Properties of Metal–Molecule–Metal Junctions Composed of 80 Oligophenylene Dithiol Molecules. *J. Am. Chem. Soc.* **2017**, *139*, 5696–5699.
- (14) Tefashe, U. M.; Nguyen, Q. V.; Lafolet, F.; Lacroix, J. C.; McCreery, R. L. Robust Bipolar Light Emission and Charge Transport in Symmetric Molecular Junctions. *J. Am. Chem. Soc.* **2017**, *139*, 7436–7439.
- (15) Nguyen, Q. v.; et al. Control of Rectification in Molecular Junctions: Contact Effects and Molecular Signature. *J. Am. Chem. Soc.* **2017**, *139*, 11913–11922.
- (16) Li, L.; Lo, W.-Y.; Cai, Z.; Zhang, N.; Yu, L. Proton-Triggered Switch Based on a Molecular Transistor with Edge-on Gate. *Chem. Sci.* **2016**, *7*, 3137–3141.
- (17) Jia, C.; et al. Covalently Bonded Single-Molecule Junctions with Stable and Reversible Photoswitched Conductivity. *Science* **2016**, *352*, 1443–1445.
- (18) Yuan, L.; Nerngchamnong, N.; Cao, L.; Hamoudi, H.; del Barco, E.; Roemer, M.; Sriramula, R. K.; Thompson, D.; Nijhuis, C. A. Controlling the Direction of Rectification in a Molecular Diode. *Nat. Commun.* **2015**, *6*, 6324–6324.
- (19) Kim, B.; Choi, S. H.; Zhu, X. Y.; Frisbie, C. D. Molecular Tunnel Junctions Based on Π-Conjugated Oligoacene Thiols and Dithiols between Ag, Au, and Pt Contacts: Effect of Surface Linking Group and Metal Work Function. *J. Am. Chem. Soc.* **2011**, *133*, 19864–19864.
- (20) Seo, K.; Lee, H. Molecular Electron Transport Changes Upon Structural Phase Transitions in Alkanethiol Molecular Junctions. *ACS Nano* **2009**, *3*, 2469–2469.
- (21) Malen, J. A.; Doak, P.; Baheti, K.; Tilley, T. D.; Segalman, R. A.; Majumdar, A. Identifying the Length Dependence of Orbital Alignment and Contact Coupling in Molecular Heterojunctions. *Nano Lett.* **2009**, *9*, 1164–1164.
- (22) Wang, G.; Kim, T.; Jang, Y. H.; Lee, T. Effects of Metal Molecule Contact and Molecular Structure on Molecular Electronic Conduction in Nonresonant Tunneling Regime: Alkyl Versus Conjugated Molecules. *J. Phys. Chem. C* 2008, *112*, 13010–13010.
- (23) Ho Choi, S.; Kim, B.; Frisbie, C. D. Electrical Resistance of Long Conjugated Molecular Wires. *Science* **2008**, 320, 1482–1486.
- (24) Akkerman, H. B.; Naber, R. C. G.; Jongbloed, B.; van Hal, P. A.; Blom, P. W. M.; de Leeuw, D. M.; de Boer, B. Electron Tunneling through Alkanedithiol Self-Assembled Monolayers in Large-Area Molecular Junctions. *Proc. Natl. Acad. Sci. U. S. A.* 2007, 104, 11161–11161.
- (25) Long, D. P.; Lazorcik, J. L.; Mantooth, B. A.; Moore, M. H.; Ratner, M. A.; Troisi, A.; Yao, Y.; Ciszek, J. W.; Tour, J. M.; Shashidhar, R. Effects of Hydration on Molecular Junction Transport. *Nat. Mater.* **2006**, *5*, 901–908.
- (26) Li, X.; He, J.; Hihath, J.; Xu, B.; Lindsay, S. M.; Tao, N. Conductance of Single Alkanedithiols: Conduction Mechanism and Effect of Molecule–Electrode Contacts. *J. Am. Chem. Soc.* **2006**, *128*, 2135–2141.
- (27) Wang, W.; Lee, T.; Reed, M. A. Electron Tunnelling in Self-Assembled Monolayers. *Rep. Prog. Phys.* **2005**, *68*, 523–523.
- (28) Engelkes, V. B.; Beebe, J. M.; Frisbie, C. D. Length-Dependent Transport in Molecular Junctions Based on Sams of Alkanethiols and Alkanedithiols: Effect of Metal Work Function and Applied Bias on

- Tunneling Efficiency and Contact Resistance. J. Am. Chem. Soc. 2004, 126, 14287–14287.
- (29) Holmlin, R. E.; Ismagilov, R. F.; Haag, R.; Mujica, V.; Ratner, M. A.; Rampi, M. A.; Whitesides, G. M. Correlating Electron Transport and Molecular Structure in Organic Thin Films. *Angew. Chem.* **2001**, *113*, 2378–2378.
- (30) Xie, Z.; Bâldea, I.; Smith, C. E.; Wu, Y.; Frisbie, C. D. Experimental and Theoretical Analysis of Nanotransport in Oligophenylene Dithiol Junctions as a Function of Molecular Length and Contact Work Function. *ACS Nano* **2015**, *9*, 8022–8036.
- (31) Nguyen, Q. V.; Martin, P.; Frath, D.; Della Rocca, M. L.; Lafolet, F.; Bellinck, S.; Lafarge, P.; Lacroix, J.-C. Highly Efficient Long-Range Electron Transport in a Viologen-Based Molecular Junction. J. Am. Chem. Soc. 2018, 140, 10131–10134.
- (32) Van Nguyen, Q.; Lafolet, F.; Martin, P.; Lacroix, J. C. Ultrathin Molecular Layer Junctions Based on Cyclometalated Ruthenium Complexes. J. Phys. Chem. C 2018, 122, 29069–29074.
- (33) Kong, G. D.; Kim, M.; Jang, H.-J.; Liao, K.-C.; Yoon, H. J. Influence of Halogen Substitutions on Rates of Charge Tunneling across Sam-Based Large-Area Junctions. *Phys. Chem. Chem. Phys.* **2015**, *17*, 13804–13807.
- (34) Bâldea, I. Ambipolar Transition Voltage Spectroscopy: Analytical Results and Experimental Agreement. *Phys. Rev. B: Condens. Matter Mater. Phys.* **2012**, *85*, 035442–035442.
- (35) Bâldea, I. Specific Issues Related to the Law of Corresponding States for the Charge Transport in Molecular Junctions Based on Graphene Electrodes. *Appl. Surf. Sci.* **2019**, 474, 256–261.
- (36) Bâldea, I. Important Issues Facing Model-Based Approaches to Tunneling Transport in Molecular Junctions. *Phys. Chem. Chem. Phys.* **2015**, *17*, 20217–20230.
- (37) Bâldea, I.; Xie, Z.; Frisbie, C. D. Uncovering a Law of Corresponding States for Electron Tunneling in Molecular Junctions. *Nanoscale* **2015**, *7*, 10465–10471.
- (38) Yang, Y. W.; Fan, L. J. High Resolution Xps Study of Decanethiol on Au(111): Single Sulfur-Gold Bonding Interaction. *Langmuir* **2002**, *18*, 1157–1164.
- (39) Bowers, C. M.; Rappoport, D.; Baghbanzadeh, M.; Simeone, F. C.; Liao, K.-C.; Semenov, S. N.; Żaba, T.; Cyganik, P.; Aspuru-Guzik, A.; Whitesides, G. M. Tunneling across Sams Containing Oligophenyl Groups. *J. Phys. Chem. C* **2016**, *120*, 11331–11337.
- (40) Nijhuis, C. A.; Reus, W. F.; Whitesides, G. M. Molecular Rectification in Metal-Sam-Metal Oxide-Metal Junctions. *J. Am. Chem. Soc.* **2009**, *131*, 17814–17814.
- (41) Hamoudi, H.; Prato, M.; Dablemont, C. l.; Cavalleri, O.; Canepa, M.; Esaulov, V. A. Self-Assembly of 1,4-Benzenedimethanethiol Self-Assembled Monolayers on Gold. *Langmuir* **2010**, *26*, 7242–7247
- (42) Pasquali, L.; Terzi, F.; Seeber, R.; Nannarone, S.; Datta, D.; Dablemont, C. l.; Hamoudi, H.; Canepa, M.; Esaulov, V. A. Ups, Xps, and Nexafs Study of Self-Assembly of Standing 1,4-Benzenedimethanethiol Sams on Gold. *Langmuir* 2011, 27, 4713–4720.
- (43) Salazar Alarcón, L.; Cristina, L. J.; Shen, J.; Jia, J.; Esaulov, V. A.; Sánchez, E. A.; Grizzi, O. Growth of 1,4-Benzenedimethanethiol Films on Au, Ag, and Cu: Effect of Surface Temperature on the Adsorption Kinetics and on the Single Versus Multilayer Formation. J. Phys. Chem. C 2013, 117, 17521–17530.
- (44) Jia, J.; Giglia, A.; Flores, M.; Grizzi, O.; Pasquali, L.; Esaulov, V. A. 1,4-Benzenedimethanethiol Interaction with Au(110), Ag(111), Cu(100), and Cu(111) Surfaces: Self-Assembly and Dissociation Processes. *J. Phys. Chem. C* **2014**, *118*, 26866–26876.
- (45) Pasquali, L.; Terzi, F.; Zanardi, C.; Pigani, L.; Seeber, R.; Paolicelli, G.; Suturin, S. M.; Mahne, N.; Nannarone, S. Structure and Properties of 1,4-Benzenedimethanethiol Films Grown from Solution on Au(1 1 1): An Xps and Nexafs Study. *Surf. Sci.* **2007**, *601*, 1419–1427.
- (46) Pasquali, L.; Terzi, F.; Seeber, R.; Doyle, B. P.; Nannarone, S. Adsorption Geometry Variation of 1,4-Benzenedimethanethiol Self-Assembled Monolayers on Au(111) Grown from the Vapor Phase. *J. Chem. Phys.* **2008**, *128*, 134711–134711.

- (47) Alarcón, L. S.; Chen, L.; Esaulov, V. A.; Gayone, J. E.; Sánchez, E. A.; Grizzi, O. Thiol Terminated 1,4-Benzenedimethanethiol Self-Assembled Monolayers on Au(111) and Inp(110) from Vapor Phase. *J. Phys. Chem. C* **2010**, *114*, 19993–19999.
- (48) Vericat, C.; Vela, M. E.; Benitez, G.; Carro, P.; Salvarezza, R. C. Self-Assembled Monolayers of Thiols and Dithiols on Gold: New Challenges for a Well-Known System. *Chem. Soc. Rev.* **2010**, *39*, 1805–34.
- (49) Pasquali, L.; Terzi, F.; Zanardi, C.; Seeber, R.; Paolicelli, G.; Mahne, N.; Nannarone, S. Bonding and Orientation of 1,4-Benzenedimethanethiol on Au(111) Prepared from Solution and from Gas Phase. *J. Phys.: Condens. Matter* **2007**, *19*, 305020–29.